Effect of Baseband Impedance on FET Intermodulation

James Brinkhoff, *Student Member, IEEE*, and Anthony Edward Parker, *Senior Member, IEEE*

***Abstract*—The intermodulation performance of an FET in the common-source configuration is dependent on the impedance presented to its gate and drain terminals, not only at fundamental, but also at harmonic and baseband frequencies. At baseband frequencies, these terminating impedances are usually determined by the bias networks, which may have varying impedance over the frequencies involved. This can give rise to asymmetry in two-tone intermodulation levels, and changing intermodulation levels with tone spacing, as previous studies have shown. In this paper, an FET is analyzed to gain an understanding, useful to the circuit designer, of the contributing mechanisms, and to enable the prediction of bias points and the design of networks that can minimize or maximize these effects. Compact formulas are given to facilitate this. An amplifier was tested, showing good agreement between the theoretical and measured results.**

***Index Terms*—FET amplifiers, impedance, intermodulation distortion, nonlinear distortion, Volterra series.**

I. Introduction

MANY STUDIES have reported that the intermodulation performance of an FET amplifier is affected, not only by the impedance presented to the device at the fundamental and higher harmonic frequencies, but also at baseband frequencies. The baseband frequencies are those of the modulating signals and, in a multicarrier system, the difference frequencies. The impedance at these low frequencies, hereafter called the baseband impedance, is usually determined by the bias networks. These create time constants in the circuit that are much larger than the period of the microwave carriers being amplified.

The baseband impedance may cause the intermodulation levels to be higher or lower, or even cause an asymmetry between the upper and lower intermodulation levels [1]–[3]. These effects are also observed in amplifiers operating under digital modulation schemes so that, for example, upper and lower adjacent channel power ratio (ACPR) measurements are sometimes observed to be different [4]. These phenomena are attributed to a low-frequency memory effect.

Other mechanisms leading to memory effects are temperature variation [5], [6] and trapping [7], which also may lead to changing intermodulation characteristics over the modulating-signal bandwidth. These effects result in ambiguity in specifying the linearity of an amplifier using a two-tone test. This is due to the distortion levels changing for different tone spacings. For example, the intermodulation intercept point measured with a tone spacing of 10 MHz may be significantly different from that measured with a spacing of 100 kHz. Possibly, manufacturers should give the intercept-point specifications for a variety of tone spacings spanning the bandwidths of interest. The upper and lower distortion products also often have different levels (are asymmetric), leading to the question of which value should be used.

Furthermore, memory effects in power amplifiers lead to difficulty in designing effective and wide-band predistortion linearizers [3]. They also make the extraction of a simple and accurate behavioral model for use in system simulation difficult because the familiar AM/AM and AM/PM single-tone characterizations do not account for long time constants. Much work has recently gone into producing accurate power-amplifier models that account for memory effects [8], [9].

The effects of the bias networks on intermodulation have been simulated using the harmonic-balance method and verified by measurement [2]. Harmonic balance allows simulation of complex circuits under different operating conditions, however, it does not provide an analytical understanding of the mechanisms contributing to the intermodulation. A pioneering paper [1] that provides an understanding of the effect of baseband impedance on intermodulation uses a small-signal Volterra-series analysis [10] of a simple single-node circuit. This gave conditions under which the intermodulation levels would be asymmetric. While leading to useful conclusions, it is based on a nonlinearity that is dependent on only one signal. This was extended to consider large-signal effects in two-tone and multitone situations, useful for power-amplifier design [11]. The simulation used the same single-node circuit and, in addition, the Volterra nonlinear transfer functions of an FET and bipolar junction transistor (BJT) circuit were considered. Measurements were given and shown to agree with the qualitative predictions given for real MESFET and BJT amplifiers. The study dealt comprehensively with distortion sideband asymmetry. The overall change in both intermodulation products with baseband impedance still needs to be considered.

This paper considers the Volterra-series analysis of an FET biased in the saturation region, with nonlinear gate–source capacitance and drain current. The analysis considers terms up to the third order, hence, the results are valid for an amplifier driven into weak nonlinearity. All measurements are performed with the power levels less than 10 dB below the 1-dB compression point for the device. Closed-form functions predicting distortion levels are derived, which provide a qualitative understanding of the effects. These functions are not complicated, but are able to predict the distortion accurately. Hence, they should

Manuscript received September 5, 2002; revised November 18, 2002. The work of J. Brinkhoff was supported under an Australian Postgraduate Award.

The authors are with the Department of Electronics, Macquarie University, Sydney, N.S.W. 2109, Australia (e-mail: jamesb@ics.mq.edu.au).

Digital Object Identifier 10.1109/TMTT.2003.808704

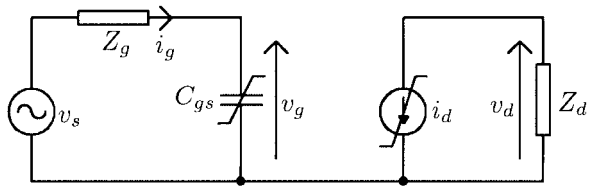

Fig. 1. FET circuit used in Volterra analysis. Note that the drain current source $i_{\rm d}$ includes transconductance, drain conductance, and cross terms, as in (1).

be useful in circuit design. The analysis considers an arbitrary input and output impedance and their effect, not only on asymmetry between intermodulation levels, but also on changes in the absolute intermodulation levels with difference frequency. This gives an understanding of the mechanisms that contribute to dependence of third-order distortion on baseband impedance, and enables prediction of bias regions and impedances that will minimize the dependence. The distortion of a pseudomorphic high electron-mobility transistor (pHEMT) amplifier was measured and compared with simulations using the derived equations, which confirmed the theory.

II. FET Circuit Analysis

In the analysis of a common-source FET operating in the saturation region, it is usual to consider two nonlinearities. The most significant is the drain current, controlled by the gate $v_{\rm g}$ and drain $v_{\rm d}$ signal voltages. The second is the gate–source nonlinear capacitance, controlled only by the gate voltage [12]. These give signal currents through the drain and gate, respectively, which can be written in a Taylor-series expansion to the third order as

$$\begin{aligned} i_{\rm d} =& G_m v_{\rm g} + G_{ds} v_{\rm d} + G_{m2} v_{\rm g}^2 + G_{md} v_{\rm g} v_{\rm d} + G_{d2} v_{\rm d}^2 \\ &+ G_{m3} v_{\rm g}^3 + G_{m2d} v_{\rm g}^2 v_{\rm d} + G_{md2} v_{\rm g} v_{\rm d}^2 + G_{d3} v_{\rm d}^3 \end{aligned} \tag{1}$$

$$i_{\rm g} = \frac{\rm d}{dt}\left(C_{gs1} v_{\rm g} + C_{\rm gs2} v_{\rm g}^2 + C_{\rm gs3} v_{\rm g}^3\right) \tag{2}$$

where the $C_{\rm gs}$ terms, defined in [12], and the G terms, defined in [13], are constants that vary with bias.

The circuit used in the analysis is shown in Fig. 1. Notice that the gate–drain capacitance is not included. This was found through simulations to have a negligible effect on the distortion results presented here. The drain–source capacitance is usually very small, but could be included in the load impedance if needed. Extrinsic elements can be accounted for in the load or source impedances as necessary. The gate is driven by a source v_s with a series frequency-dependent impedance $Z_{\rm g}(\omega)$. The drain is connected to a frequency-dependent impedance $Z_{\rm d}(\omega)$.

The analysis proceeds by finding $v_{\rm g}$ as a function of v_s using a Volterra series involving $Z_{\rm g}$ and $i_{\rm g}$. This yields the first-, second-, and third-order nonlinear transfer functions. $v_{\rm d}$ is then found as a function of $v_{\rm g}$ in terms of $Z_{\rm d}$ and $i_{\rm d}$, again giving three nonlinear transfer functions. The overall transfer functions between v_s and $v_{\rm d}$ are derived by combining the two sets of functions using a similar method to that proposed in [14]. In this case, however, the analysis is extended to consider distortion at all frequencies including baseband, instead of just the in-band products close to the carrier frequencies. The fact that out-of-band products are considered and found to contribute to in-band distortion leads to the prediction of low-frequency memory effects impacting on carrier-frequency distortion.

The result is a set of large equations for the intermodulation-distortion products, similar to those in [11], which can be simplified. A number of terms were found to be insignificant in predicting intermodulation levels at the frequencies used here and at the bias conditions of interest. These included terms that depend on the second- and third-order gate–source capacitance nonlinearity $C_{\rm gs2}$ and $C_{\rm gs3}$. However, it was found by simulation that these terms may need to be included in the model to accurately find the difference in level between the lower and upper intermodulation products at high frequencies.

If the lower and upper input tones, respectively, are at ω_1 and ω_2, then the lower and upper intermodulation products will be at $2\omega_1 - \omega_2$ and $2\omega_2 - \omega_1$. The second-order difference frequencies at $\pm(\omega_2 - \omega_1)$ are the terms that could create a memory effect. It is often assumed that the bandwidth, or frequency difference between input tones is small compared to the midband carrier frequency ω_c so that $\omega_c \approx \omega_1 \approx \omega_2 \approx 2\omega_1 - \omega_2 \approx 2\omega_2 - \omega_1$. In some cases, this narrow-band approximation is not valid, as is observed in Section III-B. The full frequency-dependent equations for intermodulation are given in the Appendix.

Assuming that the input tones and intermodulation are at frequency ω_c and that $C_{\rm gs2}$ and $C_{\rm gs3}$ can be ignored, the equations for the intermodulation levels simplify to

$$\begin{aligned} V_{d3}(2\omega_1 - \omega_2) =& V_s^3 Z_o(\omega_c) r^2 r^* \Big(c_0 Z_o(\omega_1 - \omega_2) \\ &+ c_1 + c_2 Z_o(2\omega_c)\Big) \end{aligned} \tag{3}$$

$$\begin{aligned} V_{d3}(2\omega_2 - \omega_1) =& V_s^3 Z_o(\omega_c) r^2 r^* \Big(c_0 Z_o(\omega_2 - \omega_1) \\ &+ c_1 + c_2 Z_o(2\omega_c)\Big) \end{aligned} \tag{4}$$

where

$$A = -G_m Z_o(\omega_c) \tag{5}$$

$$r = \frac{1}{1 + j\omega_c C_{gs1} Z_{\rm g}(\omega_c)} \tag{6}$$

$$Z_o(\omega) = \frac{Z_{\rm d}(\omega)}{1 + G_{\rm d} Z_{\rm d}(\omega)} \tag{7}$$

$$\begin{aligned} c_0 =& \frac{1}{2}\Big(G_{m2} + \frac{1}{2} G_{md}(A + A^*) + G_{d2} A A^*\Big) \\ &\times (G_{md} + 2G_{d2} A) \end{aligned} \tag{8}$$

$$\begin{aligned} c_1 =& -\frac{3}{4}\Big(G_{m3} + \frac{1}{3} G_{m2d}(2A + A^*) \\ &+ \frac{1}{3} G_{md2}(2AA^* + A^2) + G_{d3} A^2 A^*\Big) \end{aligned} \tag{9}$$

$$c_2 = \frac{1}{4}\left(G_{m2} + G_{md} A + G_{d2} A^2\right) \times (G_{md} + 2G_{d2} A^*). \tag{10}$$

The term A is the linear gain at the fundamental frequency ω_c. The term r is a pole due to the gate–source capacitance that reduces the levels and alters the phase of the intermodulation levels at high frequencies. The asterisk * denotes a complex conjugate, which, in this case, corresponds to negative frequency. The effective linear drain impedance is $G_{\rm d}^{-1} || Z_{\rm d}(\omega) = Z_o(\omega)$. Note that c_0, c_1, and c_2 change with

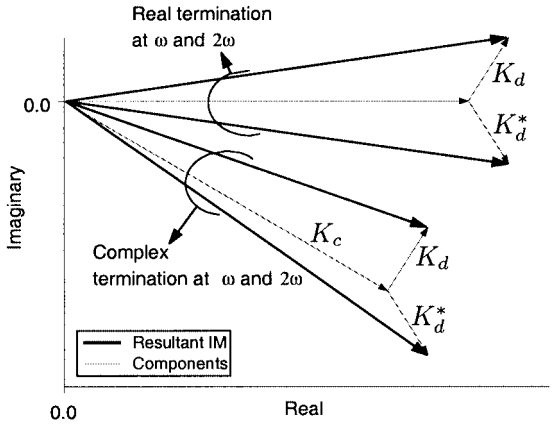

Fig. 2. Example vectors of the lower $(K_c + K_{\rm d})$ and upper $(K_c + K_{\rm d}^*)$ intermodulation products for real and complex high-frequency terminations.

bias and with output impedance at ω_c, but are independent of the difference frequency. The intermodulation dependence on third-order nonlinear terms is attributed to c_1. Intermodulation caused by second-order terms is attributed to $c_2 Z_o(2\omega_c)$ and $c_0 Z_o(\omega_1 - \omega_2)$, which involve impedances at the sum and difference frequencies.

The only difference between the expression for lower (3) and upper (4) intermodulation products is the presence of $Z_o(\omega_1 - \omega_2)$ in one and its conjugate $Z_o(\omega_2 - \omega_1)$ in the other. $Z_o(\omega_1 - \omega_2)$ is the only term in (3) that will change with the difference frequency as it is determined by the baseband impedance at the drain terminal. It is also the term that could cause a difference between the upper and lower intermodulation levels because the imaginary parts of it and its conjugate in (4) are opposite in sign.

These results can be visualized using a vector diagram of the summation in (3) and (4). Note that $K_c = c_1 + c_2 Z_o(2\omega_c)$ will be complex if the drain termination is complex at the fundamental or higher harmonic frequencies. The terms dependent on the difference frequency are defined as $K_{\rm d} = c_0 Z_o(\omega_1 - \omega_2)$ and $K_{\rm d}^* = c_0 Z_o(\omega_2 - \omega_1)$. Thus, the lower intermodulation product is proportional to $K_c + K_{\rm d}$ and the upper product is proportional to $K_c + K_{\rm d}^*$. The vector diagram shown in Fig. 2 illustrates the situations for two different drain impedances. The vectors $K_{\rm d}$ and $K_{\rm d}^*$ change with the baseband impedance. This leads to the intermodulation levels varying with different tone spacings. If the termination is real at the fundamental and second-harmonic frequencies, K_c will be at the same angle as c_0, thus, no asymmetry will be noticed. If the termination is complex, the imaginary parts of $K_{\rm d}$ and $K_{\rm d}^*$ will add to or subtract from the imaginary part K_c so that the upper and lower intermodulation products will have different magnitudes.

A number of predictions and observations are possible from the above results.

1) The variation of intermodulation with baseband impedance is dependent on the second-order drain–current nonlinearity. To correctly simulate the effect of memory on intermodulation, a model is needed that accurately predicts the second-order transconductance G_{m2}, drain conductance G_{d2}, and cross term G_{md} in (8).
2) It is possible to select a bias point and/or drain impedance such that c_0 in (3) and (4) is minimized and, hence, the dependence of the intermodulation on baseband impedance is minimized.
3) Design for minimal intermodulation distortion can be at the expense of intermodulation dependence on baseband impedance. This is not the case if the third-order terms in the drain–current nonlinearity mask the second-order terms because c_1 will dominate over c_0 in (3) and (4). However, many power-amplifier designs bias the transistors to the points of lowest intermodulation, typically where $G_{m3} \approx 0$. This will also be the point where the second-order effects are not negligible in comparison with the third-order ones. Thus, K_c will be of comparable magnitude to $K_{\rm d}$ and $K_{\rm d}^*$. This is a reason why large intermodulation changes and differences between upper and lower levels are often observed in lower intermodulation amplifiers.
4) It is the impedance of the drain termination at the difference frequency $Z_o(\omega_1 - \omega_2)$ that has the dominant effect, whereas the baseband impedance of the gate network does not have such a significant impact.
5) The intermodulation level will change with the difference in frequency between the two tones if the baseband impedance changes with difference frequency. This requires careful consideration of the frequency spacing for intermodulation testing because the intercept point can vary widely depending on the tone spacing. Also, using devices such as dc blocks at the input of a spectrum analyzer can significantly change the baseband impedance presented to the output of the device-under-test, and give uncharacteristic results to an intermodulation test.
6) The memory effect can be reduced if the baseband output impedance does not change over the desired bandwidth of operation. An obvious design that will set $c_0 Z_o(\omega_1 - \omega_2)$ in (3) to zero is one in which $Z_{\rm d}(\omega_1 - \omega_2) = 0$ over the baseband frequency range. This range must encompass the bandwidth of broad-band signals or the maximum frequency separation in a multicarrier amplifier. Thus, this design goal may not be possible in modern communication systems where large amplifier bandwidths are required.
7) A difference in the intermodulation levels will be observed if all three of the following conditions hold; they are similar to those found in [1] for a simpler system:
   - The third-order terms in the drain–current nonlinearity do not mask the second-order terms, i.e., c_1 in (3) and (4) does not dominate.
   - There is an imaginary component not much smaller than the real component in the impedance presented to the drain at either the fundamental or second-harmonic frequencies and, hence, $K_c = c_1 + c_2 Z_o(2\omega_c)$ in Fig. 2 has an imaginary component.
   - The baseband impedance $Z_o(\omega_1 - \omega_2)$ has an imaginary component not much smaller than the real component. In this case, the imaginary parts of $K_{\rm d}$ and $K_{\rm d}^*$ in Fig. 2, which are opposite in sign, will add to and subtract from the imaginary part of K_c.

This analysis has investigated the effect of baseband impedance for the simple case of two-tone intermodulation.

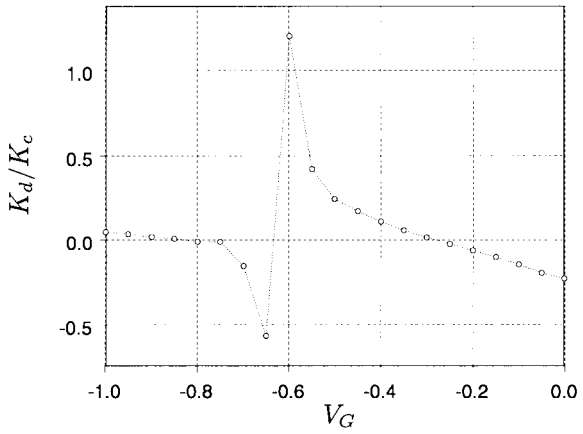

Fig. 3. Measured $K_{\rm d}/K_c$ variation with gate bias for an ATF-35143 at $V_D = 2$ V.

However, it is clear that the observations above will be true for more complex modulation schemes [4] so it should be possible to apply the same rules to predict the role of baseband impedance on the ACPR and the asymmetry between the upper and lower ACPR [11].

III. Experimental Application

A simple amplifier using an Agilent ATF-35143 packaged pHEMT was constructed to verify the above analysis. The amplifier was operated in a 50-Ω system, with a simple *LC* bias network on the gate and drain of the device.

The Taylor-series coefficients of drain current in (1) were extracted from the device using the two-tone distortion method proposed in [15]. They were extracted over gate biases from -1 to 0 V using frequencies of 50.5 and 70.5 MHz. The tones were low enough in frequency that device capacitance was insignificant. The frequencies of the tones, as well as the difference frequency, were chosen to be above the corner frequency of the bias network and any other large frequency-dispersive effects in the device such as trapping and thermal effects. The bias network consisted of a 4.7-μH inductor and a 1-nF capacitor. When this is terminated in 50 Ω, the impedance presented to the transistor by the network is approximately 50 Ω at and above 20 MHz. This is above the frequencies of any expected dispersion in the device at the drain bias of 2 V [7]. All measurements were made with an input power at -16 dBm per tone. This ensures that the device is operating in the weakly nonlinear region.

A. Effect of Gate Bias

Using the extracted Taylor-series coefficients, it is possible to predict the bias points where the baseband impedance at the drain terminal will have little effect. By examining (3) and (4), it can be seen that the baseband output impedance $Z_o(\omega_1 - \omega_2)$ is multiplied by c_0. The coefficient c_0 and, hence, $K_{\rm d}$, will vary with bias because it is dependent on the second-order drain–current nonlinearities, as seen in (8).

Fig. 3 shows the variation, as a function of gate bias, of $K_{\rm d}/K_c$, which is the ratio of the intermodulation dependent on the baseband impedance to that dependent on high-frequency impedance. The drain impedance was set at 50 Ω for the purpose of this comparison. Near $V_{\rm G} = -0.6$ V, $K_{\rm d}/K_c$ has a maximum, indicating that the baseband impedance will have a significant impact at this bias. At $V_{\rm G} = -0.3$ V, $K_{\rm d}/K_c$ is 0. As $V_{\rm G} \rightarrow 0$ V, the coefficient becomes increasingly negative. Therefore, it would be expected that the baseband drain impedance would have very little effect on the intermodulation near $V_{\rm G} = -0.3$ V, but a large effect on either side of this bias.

Shown in Fig. 4 are the measured and modeled intermodulation levels as a function of difference frequency for the three above-mentioned gate bias points. The simulated intermodulation is calculated using (3). The same level is predicted by (4) because K_c is real for the 50-Ω high-frequency impedance, thus, no asymmetry exists between the lower and upper intermodulation levels. The measurements confirmed that the magnitudes of the lower and upper intermodulation levels essentially were equal, thus, only the lower-frequency level is shown. The presence of memory effects is seen in Fig. 4 as either peaks or nulls, based on the sign of $K_{\rm d}/K_c$, as would be expected from (3). The $V_{\rm G} = -0.3$ V bias, where $K_{\rm d}/K_c \approx 0$, can be used if it is important that the intermodulation characteristics are free from memory effects. However, note that other bias points produce lower intermodulation levels over certain ranges of difference frequency.

B. Effect of Drain Impedance

The experimental amplifier was tested with a number of bias networks to investigate the relationship between the intermodulation level and drain impedance $Z_{\rm d}$ at fundamental and harmonic frequencies. Described here are the results with a real termination at fundamental and higher frequencies and the results with a complex termination at these frequencies.

Initially, the same bias network was used as in the above characterization procedure. A plot of the real and imaginary components of $Z_{\rm d}$ presented by this network at the frequencies of interest is shown in Fig. 5. The impedance at the fundamental frequency of 50 MHz is real. It is also real at higher harmonic frequencies. Therefore, no asymmetry in the intermodulation tones is expected because K_c (as in Fig. 2) is real. It can be seen that the baseband impedance changes markedly between 1–10 MHz. Below these frequencies, it presents a short circuit to the device; at higher frequencies, it is 50 Ω. Therefore, the intermodulation levels would be expected to change for tone difference frequencies in the 1–10-MHz range. This was confirmed in Fig. 4.

Initially, a bias-dependent large time constant in the power supply was not adequately bypassed and led to poor agreement in results, i.e., the impedance of the power supply is significant. This problem was eliminated and the measurements and simulations are in close agreement, the error between them being less than 1.1 dB for difference frequencies greater than 10 kHz. Below 10 kHz, there is a rise in the intermodulation levels, which may be due to the thermal effect [5]. Most importantly for this study, the simulated distortion does predict the location and direction of the peaks and nulls in the distortion caused by the external baseband drain termination. The peaks and nulls occur at around the difference frequency, where the baseband bias network impedance is changing.

For a second experiment, the bias network on the drain terminal was modified to provide an imaginary termination

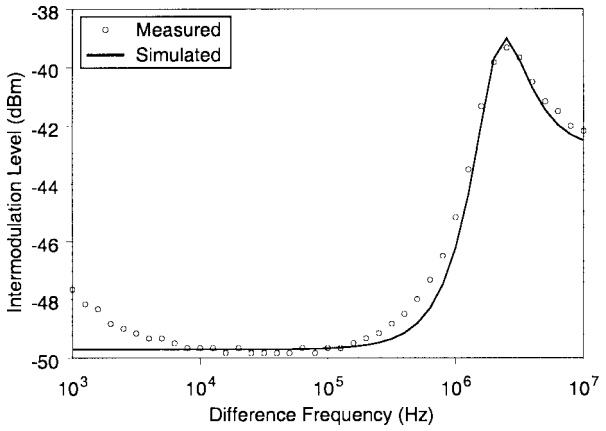

(a)

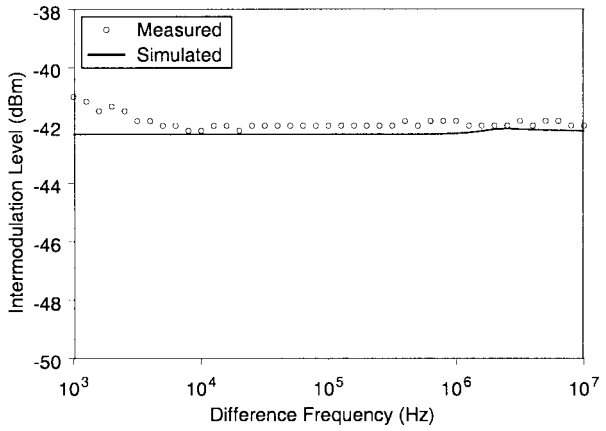

(b)

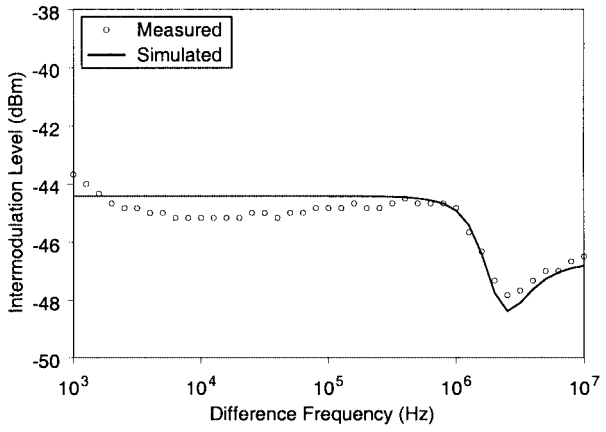

(c)

Fig. 4. Distortion measurements with real $Z_{\rm d}$ at fundamental and higher frequencies at $V_D = 2$ V. (a) $V_{\rm G} = -0.6$ V. (b) $V_{\rm G} = -0.3$ V. (c) $V_{\rm G} = 0.0$ V.

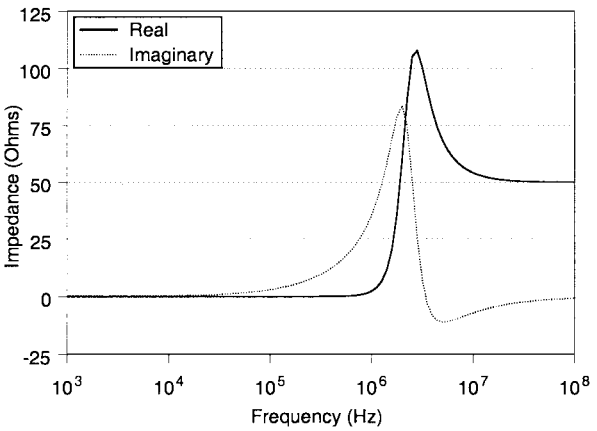

Fig. 5. Real and imaginary parts of $Z_{\rm d}$ with $L = 4.7$ μH and $C = 1$ nF in the bias network.

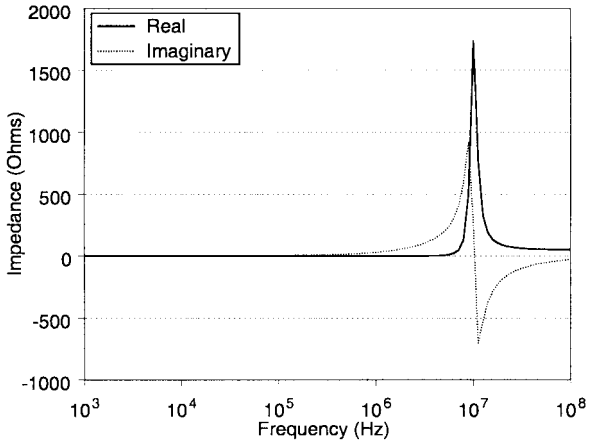

Fig. 6. Real and imaginary parts of $Z_{\rm d}$ with $L = 4.7$ μH and $C = 54$ pF in the bias network.

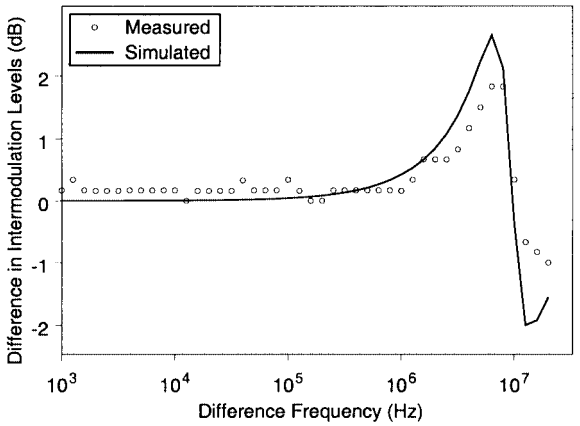

Fig. 7. Difference in intermodulation tones (lower–upper) with $Z_{\rm d}$, as in (6), for $V_{\rm G} = 0$ V, $V_{\rm DS} = 2$ V.

at the fundamental and second harmonic frequencies. The drain-bias capacitance was changed to 54 pF to achieve this. The impedance variation of the resulting $Z_{\rm d}$ is shown in Fig. 6. The imaginary component of the impedance is comparable to the real component at the fundamental frequency of 50 MHz and, hence, K_c is complex. Therefore, asymmetry in the intermodulation tones is possible when the baseband impedance has a significant imaginary component, which occurs at approximately 10 MHz. This is confirmed in a plot of the difference in intermodulation levels for $V_{\rm G} = 0$ V (see Fig. 7). The assumption that $\omega_c \approx \omega_1 \approx \omega_2$ in (3) and (4) does not give accurate results for the simulated difference in third-order levels in this case. This is because the terminating impedance is quite different at the fundamental and intermodulation frequencies for large tone spacings. Therefore, the full frequency-dependent equations given in the Appendix are used. The simulated and measured results agree fairly closely (see Fig. 7).

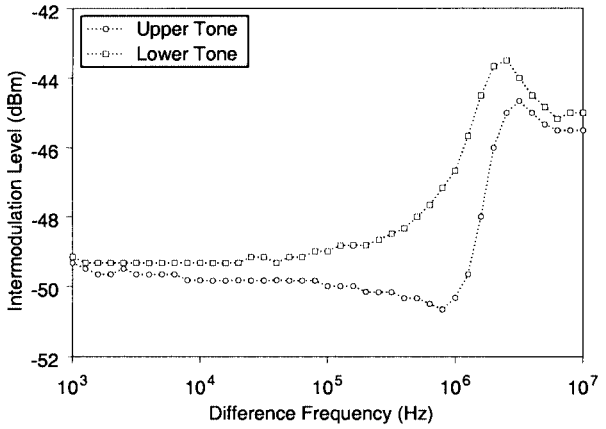

Fig. 8. Upper and lower intermodulation levels at high frequencies with $V_{\rm G} = -0.6$ V and baseband impedance, as shown in (5). The lower fundamental frequency is 2.4 GHz.

At higher frequencies, device capacitance and parasitic inductance and capacitance become significant. These were not modeled in this study. However, a graph of the measured upper and lower intermodulation levels with the lower fundamental tone at 2.4 GHz is shown in Fig. 8. This can be compared with the 50-MHz measurement at the same bias point in Fig. 4(a). The bias-network impedance in both cases is as shown in Fig. 5. The general change in intermodulation level occurs at the same difference frequency for both the low and microwave frequency measurements. This shows the general phenomenon of the change in intermodulation due to the bias network. Note that, at 2.4 GHz, there is now an asymmetry in the upper and lower levels due to K_c no longer being real. This is because the reactive elements become significant at microwave frequencies. Measurements were also carried out at $V_{\rm G} = -0.3$ V and $V_{\rm G} = 0$ V. These showed the same dependence on bias as observed in the lower frequency measurements. In particular, there was little evidence of a memory effect at $V_{\rm G} = -0.3$ V (see Fig. 4).

IV. Conclusion

This paper has demonstrated the dependence of intermodulation on an FET's baseband terminating impedance. An analytic closed-form equation has been derived to predict the third-order intermodulation products, and has been shown how to accurately predict measurements of an amplifier. This equation included the effect of baseband impedance. It is possible to predict bias points and design the networks such that intermodulation's dependence on memory effects can be optimized across the bandwidth of an amplifier. To do this, an accurate model of the FET is needed that correctly accounts for the drain–current nonlinearity dependence on gate and drain voltage, including mixing or cross terms.

Appendix

When the frequency separation in a two-tone intermodulation test is not small, the assumption that $\omega_c \approx \omega_1 \approx \omega_2$ is no longer valid. In this case, (3) and (4) may not give accurate results because the terminating impedance at ω_1 may be significantly different from the impedance at ω_2. This was noted in Section III-B. The equation for intermodulation level that does not use the above assumption is

$$v_{d3}(2\omega_p - \omega_q) = v_s^3 Z_o(2\omega_p - \omega_q) r^2(\omega_p) r(-\omega_q) \times \Big(c_0 Z_o(\omega_p - \omega_q) + c_1 + c_2 Z_o(2\omega_p) \Big) \tag{11}$$

where

$$\begin{aligned}
r(\omega) &= \frac{1}{1 + j\omega C_{gs1} Z_{\rm g}(\omega)} \\
Z_o(\omega) &= \frac{Z_{\rm d}(\omega)}{1 + G_{\rm d} Z_{\rm d}(\omega)} \\
A(\omega) &= -G_m Z_o(\omega) \\
c_0 &= \frac{1}{2}\Big[G_{m2} + \frac{1}{2} G_{md}\big(A(\omega_p) + A(-\omega_q)\big) \\
&\quad + G_{d2} A(\omega_p) A(-\omega_q) \Big] \Big[G_{md} + 2 G_{d2} A(\omega_p) \Big] \\
c_1 &= -\frac{3}{4}\Big[G_{m3} + \frac{1}{3} G_{m2d}\big(2A(\omega_p) + A(-\omega_q)\big) \\
&\quad + \frac{1}{3} G_{md2}\big(2A(\omega_p) A(-\omega_q) + A^2(\omega_p)\big) \\
&\quad + G_{d3} A^2(\omega_p) A(-\omega_q) \Big] \\
c_2 &= \frac{1}{4}\Big[G_{m2} + G_{md} A(\omega_p) + G_{d2} A^2(\omega_p) \Big] \\
&\quad \times \Big[G_{md} + 2 G_{d2} A(-\omega_q) \Big].
\end{aligned}$$

Assuming that $\omega_1 < \omega_2$, the lower intermodulation product is calculated using $p = 1$ and $q = 2$. The upper product is calculated with $p = 2$ and $q = 1$.

Acknowledgment

The authors thank the Commonwealth Scientific and Industrial Research Organization (CSIRO) Telecommunications and Industrial Physics, Sydney, N.S.W., Australia, and Dr. J. W. Archer, CSIRO, for their support.

References

[1] N. Borges De Carvalho and J. C. Pedro, "Two-tone IMD asymmetry in microwave power amplifiers," in *IEEE MTT-S Int. Microwave Symp. Dig.*, 2000, pp. 445–448.

[2] Y. Wang, S. V. Cherepko, J. C. M. Hwang, F. Wang, and W. D. Jemison, "Asymmetry in intermodulation distortion of HBT power amplifiers," in *IEEE GaAs Integrated Circuits Dig.*, 2001, pp. 201–204.

[3] J. Vuolevi, J. Manninen, and T. Rahkonen, "Cancelling the memory effects in RF power amplifiers," in *IEEE Int. Circuits and Systems Symp.*, 2001, pp. 57–60.

[4] J. F. Sevic, K. L. Burger, and M. B. Steer, "A novel envelope-termination load-pull method for ACPR optimization of RF/microwave power amplifiers," in *IEEE MTT-S Int. Microwave Symp. Dig.*, 1998, pp. 723–726.

[5] P. M. McIntosh and C. M. Snowden, "The effect of a variation in tone spacing on the intermodulation performance of class A and class AB HBT power amplifiers," in *IEEE MTT-S Int. Microwave Symp. Dig.*, 1997, pp. 371–374.

[6] N. Le Gallou, J. M. Nebus, E. Ngoya, and H. Buret, "Analysis of low frequency memory and influence on solid state HPA intermodulation characteristics," in *IEEE MTT-S Int. Microwave Symp. Dig.*, 2001, pp. 979–982.

[7] A. E. Parker and J. G. Rathmell, "Novel technique for determining bias, temperature and frequency dependence of FET characteristics," in *IEEE MTT-S Int. Microwave Symp. Dig.*, 2002, pp. 993–996.

[8] H. Ku, M. D. Mckinley, and J. S. Kenney, "Extraction of accurate behavioral models for power amplifiers with memory effects using two-tone measurements," in *IEEE MTT-S Int. Microwave Symp. Dig.*, 2002, pp. 139–142.
[9] P. M. Asbeck, H. Kobayashi, M. Iwamoto, G. Hanington, S. Nam, and L. E. Larson, "Augmented behavioral characterization for modeling the nonlinear response of power amplifiers," in *IEEE MTT-S Int. Microwave Symp. Dig.*, 2002, pp. 135–138.
[10] S. A. Maas, *Nonlinear Microwave Circuits*. Norwood, MA: Artech House, 1988.
[11] N. B. De Carvalho and J. C. Pedro, "A comprehensive explanation of distortion sideband asymmetries," *IEEE Trans. Microwave Theory Tech.*, vol. 50, pp. 2090–2101, Sept. 2002.
[12] J. A. Garcia, A. M. Sanchez, J. C. Pedro, N. Borges De Carvalho, A. T. Puente, and J. L. Garcia, "Characterizing the gate-to-source nonlinear capacitor role on GaAs FET IMD performance," *IEEE Trans. Microwave Theory Tech.*, vol. 46, pp. 2344–2355, Dec. 1998.
[13] J. C. Pedro and J. Perez, "Accurate simulation of GaAs MESFET's intermodulation distortion using a new drain–source current model," *IEEE Trans. Microwave Theory Tech.*, vol. 42, pp. 25–33, Jan. 1994.
[14] S. A. Maas, "Third-order intermodulation distortion in cascaded stages," *IEEE Microwave Guided Wave Lett.*, vol. 5, pp. 189–191, June 1995.
[15] G. Qu and A. E. Parker, "New model extraction for predicting distortion in HEMT and MESFET circuits," *IEEE Microwave Guided Wave Lett.*, vol. 9, pp. 363–365, Sept. 1999.

James Brinkhoff (S'02) was born in 1979. He received the B.E. degree from the University of Tasmania, Tasmania, Australia, in 2001, and is currently working toward the Ph.D. degree at Macquarie University, Sydney, N.S.W., Australia.

His honors project investigated the use of SiGe HBTs for wide-band low-noise amplifiers. His research interests include monolithic microwave integrated circuit (MMIC) design, effects of microwave circuit nonlinearity on communication systems, amplifier linearization, and nonlinear circuit analysis.

Anthony Edward Parker (S'84–M'84–SM'95) received the B.Sc., B.E., and Ph.D. degrees from The University of Sydney, Sydney, Australia, in 1983, 1985, and 1992, respectively.

In 1990, he joined Macquarie University, Sydney, Australia, where he is currently the Head of the Electronics Department. He is involved with a continuing project on pulsed characterization of microwave devices and design of low-distortion communications circuits. He has worked as a consultant with several companies including M/A-COM, Lowell, MA, and Agilent Technologies Inc., Santa Rosa, CA. He has developed accurate circuit simulation techniques, such as used in the Parker–Skellern FET model. He authored or coauthored over 90 publications.

Prof. Parker is a member of the Institution of Telecommunications and Electronic Engineers, Australia. He served on the Technical Committees for the 2000 IEEE Asia–Pacific Microwave Conference, Sydney, Australia, and as technical co-chair for the 2001 IEEE Symposium on Circuits and Systems, Sydney, Australia.